Beamtests of the N-on-n Silicon Microstrip Detector with Various P-stop Structures

Y. Unno[a], H. Kitabayashi[b], B. Dick[g], T. Dubbs[j], A. Grillo[j], M. Ikeda[b], Y. Iwata[b], S. Kashigin[j], E. Kitayama[h], W. Kroeger[j], T. Kohriki[a], T. Kondo[a], G. Moorhead[g], D. Morgan[k], I. Nakano[h], T. Ohmoto[b], T. Ohsugi[b], P.W. Phillips[i], J. Richardson[1,f], W. Rowe[j], H.F.-W. Sadrozinski[j], K. Sato[b], J. Siegrist[e], E. Spencer[j], H. Spieler[e], R. Takashima[d], G. Taylor[g], S. Terada[a], T. Umeda[h], M. Wilder[j], K. Wyllie[c], and H. Yagi[h]

[a]Institute of Particle and Nuclear Studies, KEK, Oho 1-1, Tsukuba 305-0801, Japan
[b]Department of Physics, Hiroshima University, Kagamiyama 1-3-1, Higashi-Hiroshima 739-8526, Japan
[c]Cavendish Laboratory, University of Cambridge, Madingley Road, Cambridge CB3 0HE, United Kingdom
[d]Department of Education, Kyoto University of Education, Fukakusa, Fushimi-ku, Kyoto 612-0863, Japan
[e]Physics division, Lawrence Berkeley National Laboratory (LBNL), 1 Cyclotron Road, Berkeley, California 94720, U. S. A.
[f]Department of Physics, University of Liverpool, P. O. Box 147, Liverpool L69 7ZE, United Kingdom
[g]School of Physics, University of Melbourne, Parkville, Victoria 3052, Australia
[h]Department of Physics, Okayama University, Tsusima-naka 3-1-1, Okayama 700-8530, Japan
[i]Particle Physics Department, Rutherford Appleton Laboratory (RAL), Chilton, Didcot, Oxon OX11 0QX, United Kingdom
[j]Institute for Particle Physics (SCIPP), University of California, Santa Cruz, California 95064, U. S. A.
[k]Department of Physics, University of Sheffield, Sheffield S3 7RH, United Kingdom

Abstract

A Silicon microstrip detector with n-strip readout on the n-bulk Silicon has been fabricated by implementing 4 different p-stop structures in 6 zones in the detector's n-side. The detectors were assembled into the units of detector-electronics modules. The response difference in the p-stop structures and effect of detector strip length were characterized in the laboratory and under the beamtests with charged pions.

I. INTRODUCTION

Silicon microstrip detectors are successfully used in the high energy physics experiments [1]. In the future experiments, such as in the Large Hadron Collider (LHC) at CERN, the Silicon microstrip detectors is planned to be a central device for tracking the charged particles in the flash of interactions. The environment for the detector is incomparable to the present experiments: the number of charged and neutral particles generated in the interactions is so large, e.g., a few times 10^{14} particles per cm^2 being accumulated over the lifetime of the device, that the radiation damage to the detector is becoming an critical issue in the development of the Silicon microstrip detectors for the experiments in the LHC [2].

The Silicon microstrip detectors are reversely biased in order to deplete the Silicon bulk to be sensitive to the passing charged particles. The radiation damage to the Silicon microstrip detectors are widely studied and the major effects are summarized in three categories: (1) Increase of the leakage current, (2) Bulk type mutation, in which the acceptor-like states are generated in the Silicon bulk, and the bulk type is mutating from the initial n-type to the p-type. The reverse bias voltage to deplete the Silicon bulk is increasing along the accumulation of the passing particles, and (3) Charge-up of the Silicon surface, which affects the electric field near the strips which are providing the electric field to deplete the detector and to collect the electrons or holes liberated by the passing charged particles [3].

The second category is also called as "type-inversion". Because of this type-inversion, the p-n junction moves from the p-side to the n-side in the initially n-bulk Silicon. The depleted region when the reverse bias voltage is applied is developing from the p-n junction. The detector initially reading out the n-side strips on the n-bulk silicon is becoming the detector reading out from the p-n junction after the type-inversion and has potential to operate the detector with partially depleted mode when depleting the bulk fully is becoming difficult.

A subtlety of the n-strip readout on the n-bulk Silicon detector (n-on-n detector) is the isolation of the n-strips in the Silicon surface. The Silicon surface is fabricated to be covered with Silicon dioxide for protection, called as "passivation". The interface of the Silicon and the Silicon dioxide is known to be charged up positively after the processing (called "built-in charge-up"). This positive charges attract the conduction electrons near the Silicon surface (forming the "accumulation layer") and shorts the n-strips. In order to cut this conductive layer, p-impurity is implanted in the surface, e.g., with lithographed patterns. This p-implant pattern, called "p-stop structure" in this paper, is not only required in the initial detector but also in the heavily damaged detector because of the surface charge-up due to the radiation damage (category (3)).

Since the p-stop structure has a finite conductivity, it introduces a coupling between the n-strips. In addition, the p-stop structure is electrically floating and its voltage-potential is determined by the electric field. If there is a defect in the edge of the n-strips or the p-stop structure, the electric field is deformed and, if the p-stop structure is continuous, the potential of the p-stop structure is determined by the potential of the defect location which might be undesirable in cases. A variety of p-stop structures are proposed and fabricated in the Silicon microstrip detectors for studies presented in this paper.

---

[1]Present address: Physics division, LBNL

Another interesting aspect associated with the readout of the Silicon microstrip detectors is the effect of the resistance of the metal electrode which is capacitively coupled to the n-strips implanted [4]. A resistance connected to the input of amplifier generates electronic noise due to the thermal agitation. In this study, two Silicon microstrip detectors are electrically connected in two configurations: (1) Reading out from the end of the strips (End-tap configuration); the effective strip resistance becomes twice, and (2) Reading out from the centre of the strips (Centre-tap configuration); the effective strip resistance becomes half, thus the ratio of the two resistances is 4.

II. DETECTOR

A. N-on-n detector, nn80AC

Large area n-on-n Silicon microstrip detectors were fabricated out of 4-inch silicon wafers. The outer dimension of the detector was 63.6 mm (width) and 64.0 mm (length). The silicon strip detector was a single-sided readout one and named as "nn80AC" since the detector had n-strips on n-bulk, a strip pitch of 80 μm, and an AC coupling readout configuration. The specification of the detector is summarized in Table 1. The detector had 768 readout strips divided into 6 zones with 128 strips per zone. The zones had combinations of p-stop structure and width of readout metal as listed in Table 2. Zones from 1 to 4 had the same strip and metal width but different p-stop structures. Zones from 4 to 6 had the same p-stop structure but different metal widths.

Table 1.
Specification of n-on-n single-sided silicon strip detector (nn80AC)

Detector type:	N-bulk, n-strip, AC-coupled, Single-sided
Bulk:	N-bulk, 300 μm thick
Resistivity:	4~8 kΩcm
Size (Outer):	6.36 cm × 6.4cm (width × length)
N-sensitive area:	Width: 770 × 80μm =61.6 mm
	Length: 62 mm
P-side structure:	DC-coupled pad
	Junction breakdown ≥300V
Surface protection	SiO_2 passivation
Number of N-strips:	(128 × 6 zones=768 readouts)+2 dummies
N-strip isolation:	Various p-stop structures (Table 2)
N-strip parameters:	
Polysilicon bias resistor:	1.5±0.5 MΩ
Strip pitch:	80 μm
Readout pitch:	80 μm
Implant width:	16 μm
Width of Al metal:	16 μm, and others (Table 2)
P-stop width:	43 μm, and others (Table 2)
Al thickness:	1.5 μm
Resistance of Al metal:	≤20 Ω/cm
Resistance of implant:	≤100kΩ/cm
AC-coupling:	SiO_2 0.25μm+SiN 0.05μm

Table 2.
N-implant and p-stop widths in the various p-stop structures

Zone	P-stop structure	Metal [μm]	P-stop [μm]	No. strips
1	Slit-common	16 μ	2 x 18 μ	128
2	Individual	16 μ	2 x 18 μ	128
3	Combined	16 μ	2 x 11 μ + 6 μ	128
4	Full-common	16 μ	44 μ	128
5	Full-common	22 μ	44 μ	128
6	Full-common	10 μ	44 μ	128

The detector, p-stop structures, and strip widths are abstracted schematically in Figure 1. The p-stop structures were named as Zone 1 (Slit-common), 2 (Individual), 3 (Combined), and 4, 5, 6 (Full-common). The major variation was the Full-common and the Individual p-stop structures. The secondary variation came from the point of view that in the Individual p-stop structure there still was a continuously conductive accumulation layer surrounding the p-stop structure. In order to interrupt this continuous layer, the Individual p-stop structures were sectioned into bays with an additional p-stop frame, forming the combination of the Full-common and the Individual p-stop structures (the Combined p-stop structure). The last was the Slit-common where the short p-lines are connecting the Individual p-stop structures to the surrounding p-frame.

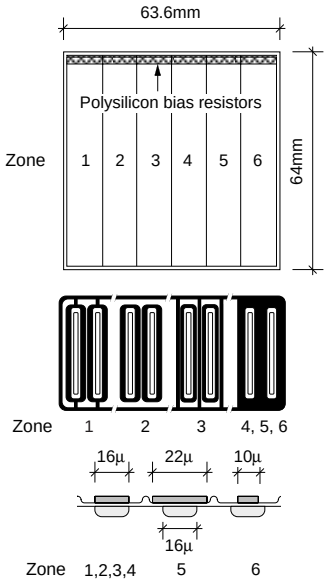

Figure 1: Schematic diagram of the n-side of the detector. Top: Detector and Zone numbers, Middle: Concept of the p-stop structures, Bottom: Widths of the n-implant strips and of the AC-coupling metal electrodes.

B. Detector-Electronics module:-- End-tap

In order to measure the response of the detector, such as

noise, efficiency, charge collection, etc., two “modules” were constructed using the detectors and a set of Application Specific Integrated Circuits (ASIC’s), LBIC for the preamplification, shaping, and on-off discrimination, and CDP for buffering the on-off binary bits [5]. The LBIC had an unipolar shaping with a peaking time of order of 20 ns which was matching the bunch crossing of 25 ns in the LHC.

One type of module, End-tap, was made by placing the readout hybrids made of Copper-Kapton at the end of the detectors as shown in Figure 2. The hybrids were glued on an extension of the baseboard discussed in the following. A pitch-adapting “Fan-in” was used to match the strip pitch of 80 μm and the pad pitch of 43 μm of LBIC’s.

The module was fabricated out of four nn80AC detectors to form double-side readout configuration. Two pairs of two detectors were glued on top and bottom of a heat conducting baseboard. Two detectors on one side were daisy-chained to make a strip length of 12 cm. The bottom detectors were rotated by 40 mrad relative to the top ones to make stereo measurement of the positions of passing charged particles; the top side was called the “axial” and the bottom the “stereo” side.

The heat conducting baseboard is critical in designing the module for the LHC since the leakage current is so large that the detector will fall into the thermal runaway unless they are properly cooled. The baseboard of the module was prototyped with a pyrolytic graphite (PG700) which had a high thermal conductivity, about 300 W/m/K [6]. The module was attached to an external PC board which also carried electronics to transmit and receive the signals over 20 m distance between the modules and the backend electronics.

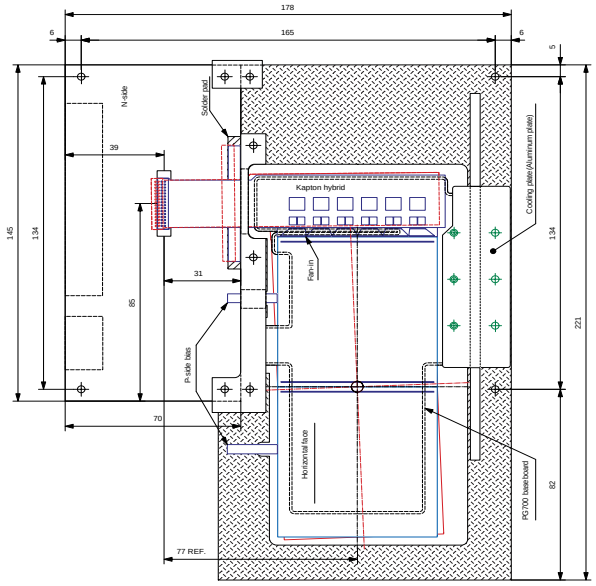

Figure 2: Overall view of “End-tap” module supported on a PC board. The strips of the front detectors run vertically (axial side) and the back detectors (stereo-side) were rotated 40 mrad to the front detectors.

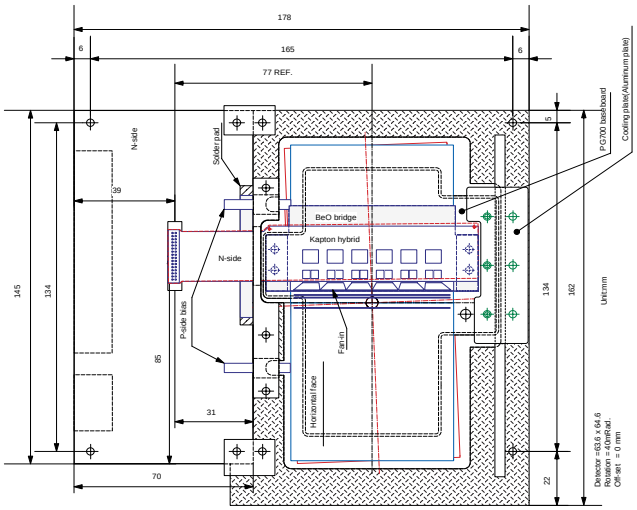

Figure 3: Overall view of “Centre-tap” module supported on a PC board. The strips of the front detectors run vertically (axial side) and the back detectors (stereo-side) were rotated 40 mrad to the front detectors.

III. Laboratory Measurements

Evaluation of the detectors was done in the laboratory and in the accelerator, using negatively charged pions produced from the 12 GeV proton synchrotron at KEK. Laboratory measurements were suited for evaluating the basic characteristics, such as the capacitance and the electronic noise, but only the charged particles from accelerators gave the controlled response in the detector.

A. Interstrip capacitance of nn80AC detector

In order to characterize and compare the zones, capacitance between the strips, so-called “interstrip capacitance”, was measured for one strip against neighbouring 12 strips per side, i.e., 24 strips in total, in a stand-alone detector. The strip length was 6.2 cm. The results for Zones, from 1 to 4, are shown in Figure 4. The measurement was done at the frequency of 1 MHz and estimated at most to have an systematic error of 0.5 pF.

A strong change of the interstrip capacitance was observed below the bias voltage of 60 V. This was an indication that the

C. Detector-Electronics module:-- Centre-tap

The other type of module, Centre-tap, was made by placing the readout hybrids near the middle of the detectors as shown in Figure 3. In this module, the Copper-Kapton hybrids were glued on a bridge, made of BeO ceramics, which was crossing over the detector with a clearance between the detector and the bridge of several hundred microns. The ends of the bridge were glued on the extended edges of the baseboard. This bridging was made to avoid any damage to the detector by gluing the hybrid.

n-side was shorted because of the undepleted region near the surface. Above this bias voltage, although the interstrip capacitances were flattened, they did not show saturation even at 200 volts. Two sources were thought responsible for the slow decrease: (1) one was the p-stop structure, and (2) the remaining electron-accumulation layer between the n-strips. An excess electric field was required to deplete the p-stop structures and to repel the electrons in the accumulation layer. Apart from the global behaviour, the Individual and the Combined p-stop structures had the least interstrip capacitance.

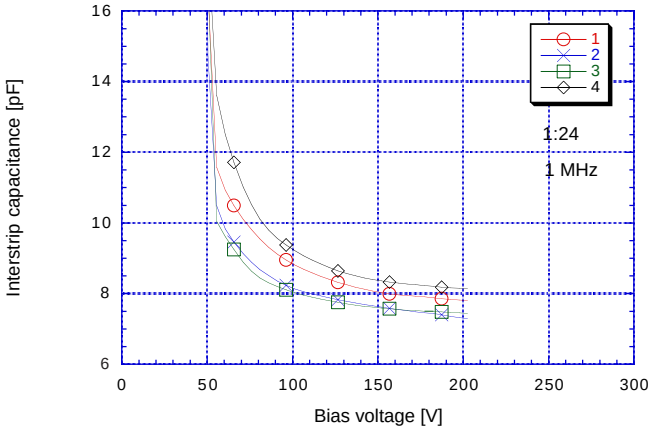

Figure 4: Inter-strip capacitances in Zones 1 (Slit-common), 2 (Individual), 3 (Combined), and 4 (Full-common), measured at 1 MHz and 1 strip against neighbouring 24 strips. The slow decrease of the capacitance above 60 volts is a reflection of conductive layer between the n-strips.

B. Noise occupancy

With the fabricated modules, two results were extracted: (1) the noise occupancy in Zones, and (2) the noise occupancy in the End-tap and the Centre-tap configurations. Noise occupancy was the hit rate in a strip due to the electronic noise of the amplifier. For high enough thresholds of the discriminator the occupancy, Π, was the measure of the noise in the tail of noise-Gaussian distribution integrated over the threshold, approximated as

$$\Pi \approx \exp(-(threshold)^2/(2\sigma^2)) . \quad (1)$$

When the occupancy was plotted in semi-log graph with the horizontal axis in (threshold)^2, the occupancy followed the straight line with the slope expressing the root-mean-square (RMS) noise.

The occupancy as the function of the threshold squared was obtained at the bias voltage of 200 V as shown in Figure 5 for the Centre-tap module. A similar result was obtained for the End-tap module, and the extracted RMS noises were summarized in Table 3. There was no data in Zone 4 of the Centre-tap module because of the dead chip. The difference of the zones and of the readout configuration was highlighted in Figure 6, where the occupancy at 1 fC threshold was shown.

The major contribution to the noise was the input capacitances connected to the input of the amplifier to which the largest contribution was the interstrip capacitance. The RMS noises and the occupancies were consistent with the interstrip capacitances shown in Figure 4, although the difference of the interstrip capacitances of the Individual and the Combined p-stop structures were not as large as the difference of the noise occupancies. The fractional increase in the RMS noise, of order of 6% for most of the zones, were observed in the End-tap configuration over the Centre-tap one, which was consistent with the expectation presented in the reference [4].

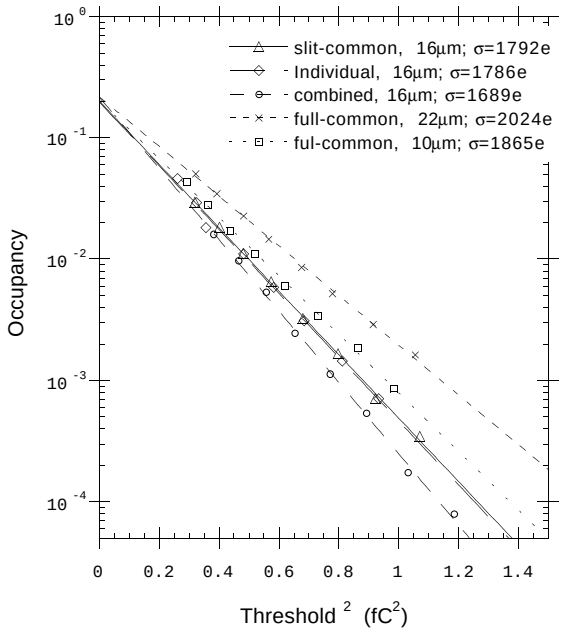

Figure 5: Average noise occupancy for the zones of the Centre-tap module as a function of the threshold squared. Inset in the figure is the RMS noises extracted from the slopes of the fitted curves.

Table 3.
RMS noises for Zones in End- and Centre-tap modules

Zone	P-stop structure	Metal [μm]	RMS noise [e]		Fractional increase [%]
			End-tap	Centre-tap	
1	Slit-common	16 μ	1908	1792	6
2	Individual	16 μ	1895	1786	6
3	Combined	16 μ	1740	1689	3
4	Full-common	16 μ	1982	---	---
5	Full-common	22 μ	2026	2024	0
6	Full-common	10 μ	1988	1865	7

IV. BEAMTESTS USING PION BEAMS

Two beamtests were carried out at KEK at the π2 beamline of the 12 GeV proton synchrotron. Negatively charged pions with a momentum of 4 GeV/c were swept over the zones of the End-tap and the Centre-tap modules [7]. The beam profile at the modules was about 1 cm in the full-width-half-maximum

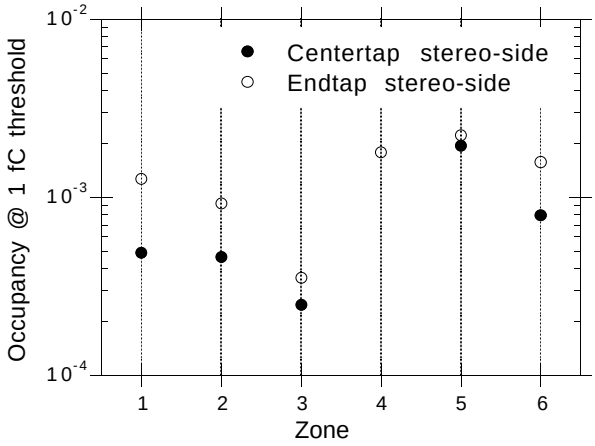

Figure 6: Noise occupancy at 1 fC threshold for Zones of both the End-tap and the Centre-tap modules.

(FWHM) horizontally and vertically, and an intensity of 1k pions per cm^2. The data-taking (DAQ) rate was about 150 events over the beam spill of 2 sec in the beam cycle of 4 sec, limited by the DAQ capability.

A. Setup

The setup in the beamtests is displayed in Figure 7. The two modules, often called "device-under-test (DUT)", were sandwiched between high precision silicon-strip detector "telescopes" (Si-telescope). The distance between the telescopes was about 60 mm and the two modules were placed at nearly equal spacing. Incident particles were triggered by coincidence of three scintillation counters, each of which had an area of 20 mm x 20 mm.

Each Si-telescope module was made of two single-sided strip detectors with their strips in orthogonal directions: one was in the horizontal direction, X, and the other in the vertical direction, Y. The silicon-strip detector was made of an implant strip pitch of 25 μm and a readout pitch of 50 μm. The sensitive region was 19.2 mm x 19.2 mm with a number of readout channels being 384. The spatial resolution was about 5 μm using the pulse height information from the strips [8].

The pion beams were set to hit the DUT's in the normal incidence. The full 6 zones were covered by 3 positions of the Si-telescopes by moving the DUT's relative to the Si-telescopes.

Data were collected at bias voltages of 80, 120, 160, and 200 volts. The threshold voltage of the discriminator was varied to have a set of 0.6, 0.8, 1.0, 1.1, 1.2, 1.3, 1.4, 1.5, 1.6, 1.8, 2.0, 2.5, 3.0, and 3.5 fC in threshold when expressed in the unit of charge according to a common calibration curve.

B. Results

1) Responses in the strip and in the midway regions

An example of efficiency variations as a function of threshold is shown in Figure 8. The figure included three cases: (1) efficiencies without specifying the beam hit positions between the

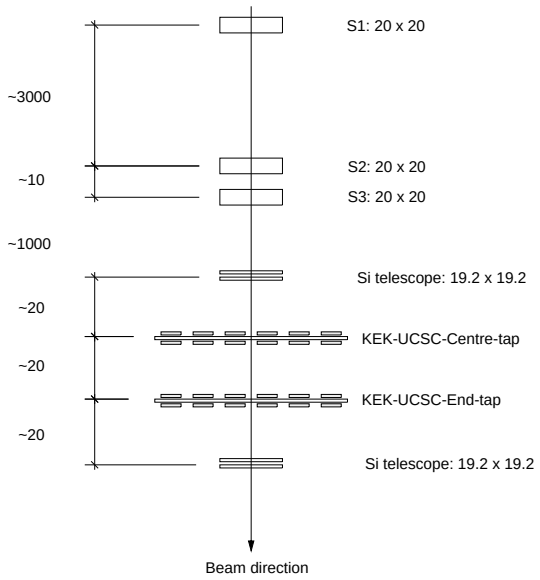

Figure 7: Setup of the DUT's, the Si-telescopes, and the scintillation counters for triggering.

strips (all region), (2) efficiencies for the tracks near the strip region (strip region), and (3) efficiencies in the midway between the strips (midway region). The efficiency curve is the integral of pulse height distribution, called "Landau distribution", above the thresholds. The threshold of 50% efficiency is corresponding to the median pulse height of the collected charges in one strip.

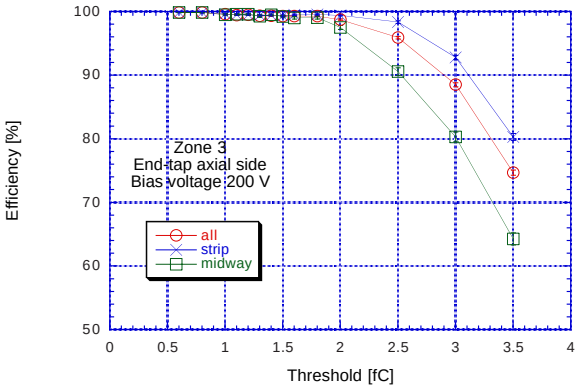

Figure 8: An example of the efficiency variation as a function of the threshold in the all (circle), the strip (cross) and the midway (square) regions. The curves drawn in the figures are simple connections of data points.

The charge collection near the strip region is expected to be similar to the planar diode case, while in the midway region the charge is expected to split into two adjacent strips. In order to define the strip region, the efficiency for detecting particles was mapped out between adjacent two readout strips. The detection

efficiency was defined by counting the existence of hit-strips within ±250 μm from the position of a track interpolated from the Si-telescope hits. An example of the plot is shown in Figure 9. The horizontal axis, Eta, was the distance from one strip to the adjacent strip normalized with the pitch of the strips.

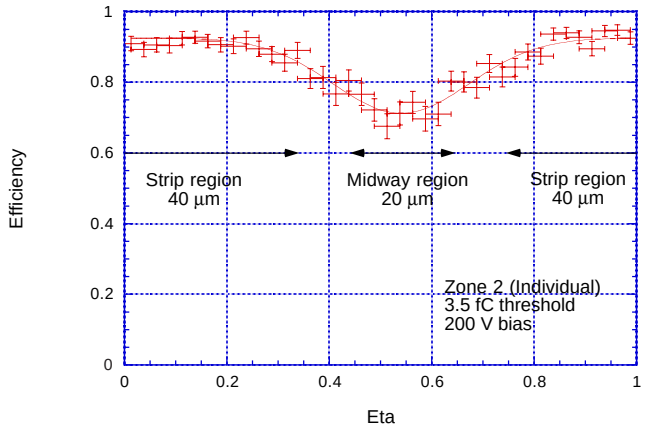

Figure 9: Efficiency as a function of "Eta", the normalized distance between adjacent two strips. The minimum was obtained by fitting Gaussian. The midway region was defined around the minimum with a full width of 20 μm. The strip region was defined around the complementary point to the minimum with a full width of 40 μm.

The loss of efficiency in the midway region was evident in the high threshold as in the figure. By fitting a Gaussian, the "midway" region was defined with a full-width of 20 μm around the minimum. The "strip" region was defined with a full-width of 40 μm around the complementary point to the minimum, which left 10 μm gap between the strip and the midway regions. The definition was made for one high threshold at 200 volts and applied to other thresholds and bias voltages uniquely.

The charge generated by a charged particle in the 300 μm thick Silicon detector is about 3.5 fC. Even applying the charge calibration chip-by-chip, the collected charges in the strip region in Zones at very high bias voltage were not satisfactorily in coincidence in these beamtests. In order to calibrate the chip dependence, the thresholds of 90% efficiency were scaled to their average, obtaining the threshold by fitting the Error function, i.e., the integral of Gaussian function as an approximation of the integral of Landau distribution, to the efficiency curves in the strip region. Although the 90% efficiency threshold is not the median, it is a parameter correlated to the median of the collected charges.

In order to quantify the loss of the collected charges in the midway region, the threshold of 90% efficiency of the midway region was divided by that of the strip region. The ratios are shown in Figure 10 for the End-tap module and at the bias voltage of 200 V. Since we took ratio, the chip dependence was being cancelled out. The statistical errors were as small as the size of the circles.

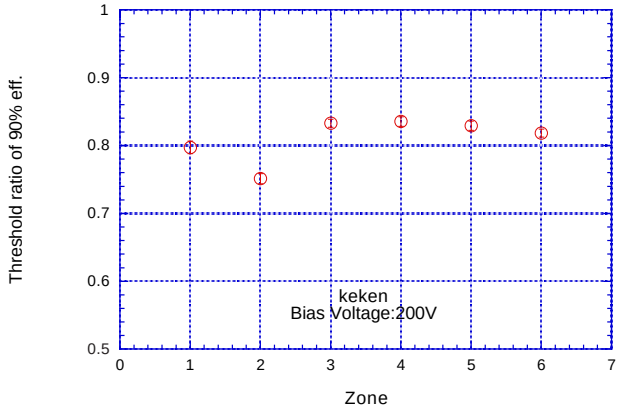

Figure 10: Ratios of the thresholds at 90% efficiency of the midway region over that of the strip region. The ratio corresponds to the ratio of collected charges in the regions.

2) Multi-strip hit fraction

If the charge collection is different in the midway region, the difference would also be reflected in the fraction of the clusters with two or more strip hits. The fraction of the multi-hit clusters were analysed and obtained to be around 14.5% at 1 fC threshold, independent of Zones. This would be understood as that the fraction was a convolution of the real fraction and the detection efficiency, and in the first order the gain in the real fraction was cancelled out with the loss in the efficiency.

3) Spatial resolutions

It was interesting to analyse the spatial resolution in different zones. A fundamental spatial resolution out of the on-off readout of strips is the (pitch/sqrt(12)), which gives 23.1 μm for the 80 μm pitch strips. Two external contributions smeared the resolution: (1) the multiple scattering contribution in this setup was about 3 μm, and (2) the Si-telescope spatial resolution was about 5 μm, thus the convoluted spatial resolution becomes 23.6 μm.

On-off readout of the strips had a built-in feature to improve the resolution; only the particles passing through the midway region induced double-strip hits, thus splitting the pitch into two narrower regions with single-strip hits and with double-strip hits.

Distances between the nearest cluster centres and the interpolated hit positions of particles from the Si-telescope were plotted for the hits in Zone 2 of the End-tap module at the bias voltage of 200 V in Figure 11. The cluster was defined as a block of contiguous hit-strips. When the hit-strip was isolated, it consisted one cluster. The cluster centre was defined as the geometrical mean of the hit-strip positions. Gaussian function was fitted to the distributions and the spatial resolutions were defined with the sigma of the Gaussian.

In the figure, the top showed the spatial resolution of the single-strip hit clusters, the middle the multi-strip hit clusters, and the bottom the all clusters. The single-strip clusters gave the spatial resolution of 23.9±0.2 μm, the multi-strip clusters

10.3±0.5 μm in the narrow peak region and 50±4 μm in the broad tail region, and the all clusters 24.7±0.2 μm. The narrow peak region in the multi-strip clusters was the hits in the midway regions while the broad tail distribution was thought to be caused by the electronic noise and associated particles with the incident ones, e.g., delta-rays. Although there was an indication of a better spatial resolution in the double-strip hit clusters, the resolution of the single-strip hit clusters was not better than the pitch/sqrt(12), and the overall resolution was slightly worse than the calculated 23.6 μm. There was little variation of the spatial resolutions in the different zones.

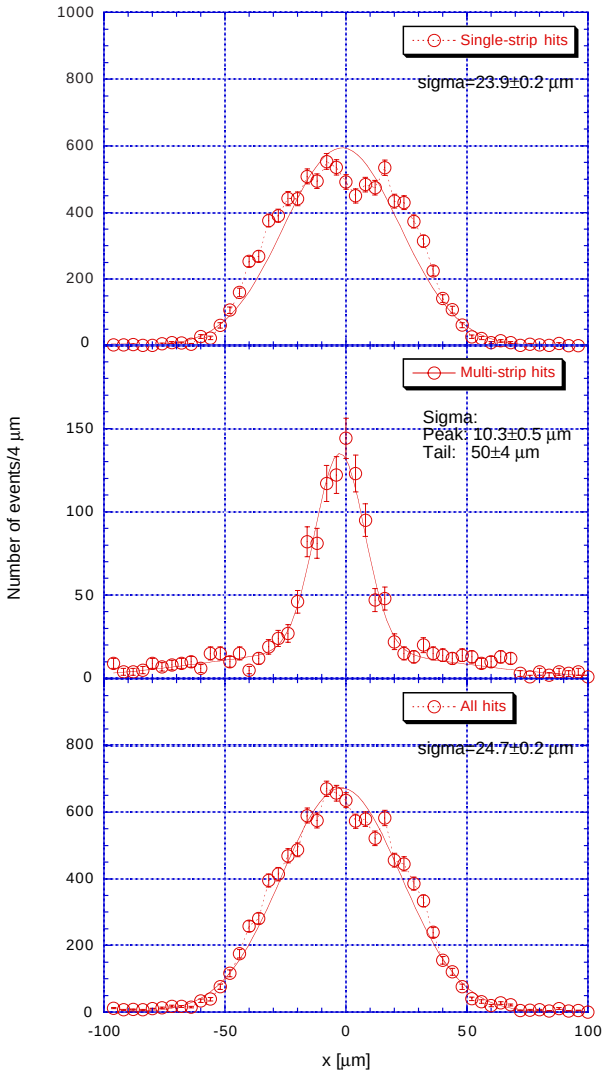

Figure 11: Spatial resolutions of the single-strip hit (top), the multi-strip hit (middle), and the all events (bottom) in Zone 2 of the End-tap module at the bias voltage of 200 V. The sigma's of the Gaussian fit are inset. A double Gaussian function was fitted to the multi-strip hits.

4) Noise occupancy

The noise occupancy in the beamtests was defined with the random hits in the strips not associated with the hits of the passing tracks. A veto-window of ±500 μm was opened around the interpolated track position in the DUT's. The occupancy was deduced by dividing the hits in the strips outside the veto-window by the number of accepted events.

The discriminator thresholds of different chips were re-scaled as mentioned earlier, using the thresholds of 90% efficiency at the bias voltage of 200 V. The occupancies obtained were plotted against the re-scaled threshold squared, as in Figure 5, straight lines were fitted, and the occupancies at 1 fC threshold were interpolated. The resulting noise occupancy at 1 fC is shown in Figure 11 for the same zones and chips shown in Figure 5.

This evaluation of the occupancy with the calibration using the beam was well in coincidence with the result obtained in the laboratory. The closeness of the occupancy in Zone 2 and 3 was reflecting the interstrip capacitance measurement more adequately. The occupancy difference in the End-tap and the Centre-tap modules was also reproduced in Zones.

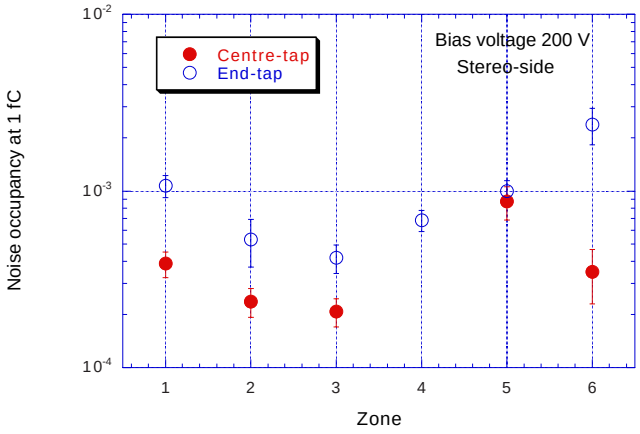

Figure 12: Noise occupancies at a threshold of 1 fC of the centre-tap (circle) and the end-tap (cross) modules measured in the beamtest.

V. SUMMARY

The Silicon microstrip detector with the n-strip readout on the n-bulk Silicon appears to be a prime candidate detector in the next generation high energy experiments, such as in the LHC, where the particle fluence is exceeding a few times 10^{14} particles per cm^2. Subtlety of the n-strip readout is the involvement of the n-strip isolation with p-implantation between the n-strips. One way of this p-implantation implementation is done with a lithographed p-pattern called the p-stop structure. A Silicon microstrip detector with n-strip readout on the n-bulk Silicon, nn80AC, was fabricated with variety of p-stop structures in the n-side in 6 zones: Slit-common, Individual, Combined, and Full-commons with 3 widths in the AC coupling electrode metal.

The detectors were characterized individually and in the units of detectors and electronics, the modules. Two types of the modules were prepared: End-tap, reading out two daisy-chained

detectors at the end of the strips, and Centre-tap, reading out at the middle of the two detectors, in order to assess the noise performance of the 4 times difference in the strip resistance, in addition.

Characterization was made in the laboratory and, subsequently, in the beamtests using charged pions generated in the 12 GeV proton synchrotron at KEK. The interstirp capacitances were measured in different zones. The Individual and the Combined p-stop structures showed the least inter-strip capacitance. The noise occupancies were measured in the two modules. The derived RMS noises and the occupancies at 1 fC threshold were consistent with the interstrip capacitance; the noise was least in the Combined p-stop structure. The RMS noise was of order 6% higher in the End-tap to the Centre-tap module, which was consistent with an prediction.

The response to the charged particle is a direct measure of the detector performance in experiment. Charged particle detection efficiencies were obtained as a function of the threshold of the electronics system, in the strip region and in the midway region between the n-strips. A loss of charge collection was observed in the midway region, and the Individual p-stop structure was observed to loose the most. This loss was understood to be caused by the existence of continuous electron accumulation layer connecting all the individual p-stop structures. The noise occupancy was measured in the beamtests and the thresholds were calibrated using the beams. The noise occupancies were basically in coincidence with those obtained in the laboratory measurement and were reinforcing the conclusion obtained.

VI. Acknowledgements

The authors wish to acknowledge J. Carter of Univ. of Cambridge, N. Jackson of Univ. of Liverpool, M. Tyndel of RAL, P. Sellin of Univ. of Sheffield, and A. Seiden of UC Santa Cruz for their strong support to the program, and the operation crews of the KEK 12 PS and its beam channels for their support to the execution of the beamtests.

This work was supported by Japan Ministry of Education, Science, and Culture, and Japan Society for Promotion of Science, US Department of Energy, Australian Department of Industry, Science and Tourism, Australian Research Council, and UK Particle Physics and Astronomy Research Council.

VII. References

[1] See, e.g., Proceedings of the Second International Symposium on Development and Application of Semiconductor Tracking Detectors, Nucl. Instr. Meth. A383, 1996

[2] ATLAS Inner Detector Technical Design Report, Vol.2, CERN/LHCC/97-17

[3] See, e.g., Review of Particle Physics, Eur. Phys. J. C3, 157-158, 1998

[4] I. Kipnis, Noise Analysis due to Strip Resistance in the ATLAS SCT Silicon Strip Module, LBNL note 39307, August 1996

[5] LBIC: E. Spencer et al., “A Fast Shaping Low Power Amplifier-Comparator Integrated Circuit for Silicon Strip Detectors”, IEEE Trans. Nucl. Scie, Vol. 42, pp. 796-802, Aug. 1995; CDP: J. DeWitt, “A Pipeline and Bus Interface Chip for Silicon Strip Detector Read-out”, Proc.IEEE Nucl. Scie. Symp., San Francisco, CA., Nov. 1993

[6] Pyrolytic graphite data sheet, Advanced Ceramics Corporation, P.O.Box 94924, Cleveland, Ohio 44101, U.S.A; In Japan: Tomoe Engineering Co. Ltd., Daini Maruzen Building, 9-2 Nihonbashi 3-Chome, Chuo-Ku, Tokyo 103, Japan

[7] T406, Participating institutions: Univ. Cambridge, Hiroshima Univ., KEK, LBNL, Univ. Liverpool, Univ. Melbourne, Okayama Univ., RAL, Univ. California Santa Cruz, Univ. Sheffield: T417, Participating institutions: Hiroshima Univ., KEK, LBNL, Univ. Melbourne, Univ. Okayama

[8] O. Toker, S. Masciocchi, E. Nygard, A. Rudge, P. Weilhammer, “Viking: A CMOS low noise monolithic 128-channel frontend for Si strip detector readout”, Nucl.Instr.Meth. A340, pp. 572-579, 1994